Available online at www.sciencedirect.com
ScienceDirect
Thermochimica Acta 453 (2007) 42–51
thermochimica acta
www.elsevier.com/locate/tca

Decomposition of tetraalkylammonium thiotungstates characterized by thermoanalysis, mass spectrometry, X-ray diffractometry and scanning electron microscopy

M. Poisot, W. Bensch *

Institut für Anorganische Chemie, University of Kiel, Olshausenstr. 40-60, 24118 Kiel, Germany

Received 9 August 2006; received in revised form 9 November 2006; accepted 9 November 2006
Available online 17 November 2006

Abstract

Thermal decomposition reactions of tetraalkylammonium thiotungstates, $(R_4N)_2WS_4$ (R = methyl to heptyl), were investigated with DSC and DTA–TG coupled with mass spectroscopy (MS). The results demonstrate that the complexity of thermal decomposition reactions is significantly influenced by the alkyl group, i.e., more complex steps are observed for the materials with longer alkyl chain lengths. Tetraethyl and tetrapropyl complexes show reversible and irreversible phase transitions detected by DSC experiments combined with thermodiffractometry. The tetrapentyl compound undergoes an irreversible phase transition while the tetraheptyl sample exhibits a glass-like transition and melting prior to decomposition. The whole series of compounds decompose without forming sulfur rich WS_n ($n = 3$ or 4) intermediates. The final WS_2 products are nearly stoichiometric for R = methyl to pentyl but for hexyl and heptyl samples the sulfur content is significantly reduced with a W/S ratio of about 1.5. The residual carbon and hydrogen contents increase in the final decomposition products in the same order as the number of C atoms in R_4N increase. For the N content no clear trend is obvious. A general thermal decomposition mechanism is suggested which follows a bimolecular nucleophilic substitution reaction. In the SEM images only for R = heptyl the formation of macro-pores with a sponge-like morphology is seen, but for the other precursors compact materials are formed which in part display a well developed morphology. X-ray diffraction analysis of the final products shows the formation of amorphous WS_2 up to the tetrapentyl precursor. But for the tetrahexyl and tetraheptyl materials the W:S ratio is significantly smaller than 1:2 and large amounts of C and H are determined by chemical analyses. In accordance with previously reported results it can be assumed that a carbosulfide phase is formed by a mixed C–W–S sandwich layered structure.

Keywords: Tetraalkylammonium thiotungstates; WS_2 preparation; Thermal decomposition; Thermoanalysis; Thermodiffractometry

1. Introduction

The increasing restrictions of environmental regulations on sulfur, nitrogen and aromatic contents of vehicle transportation fuels and by the decreasing availability of high quality crude oil deliver a lot of reports about high efficient hydrotreating catalysts. Transition metal sulfides, mainly molybdenum and tungsten disulfide, promoted with cobalt or nickel, are widely used to remove heteroelements [1–3]. Alumina is commercially used as a support because of its high surface area and its strong interaction with MoS_2, which allows good dispersion and stabilization of the active phase [1]. The current research focuses on the support material for the active sulfides. Activated carbon, TiO_2, ZrO_2, zeolites, MgO and various mixed oxides have been studied as potential alternatives for the conventional support [4–7]. Unsupported molybdenum and tungsten sulfide catalysts with high surface areas have been synthesized using thiosalts as precursors [8–12]. Cobalt promoted unsupported catalysts prepared from the decomposition of thiosalts show higher activities than the catalysts obtained by common preparation methods [13]. Some alumina supported tungsten catalysts promoted with nickel were obtained from oxy and thiosalts using fluorine as additive [14–17]. The decomposition of tetraalkylammonium thiometallates has been used to prepare WS_2 catalysts for hydrodesulfurization and the reactions were followed by DTA and TG methods [18]; however a clear mechanism of the processes has not yet been established. During the last few years the number of structurally characterized thiotungstates increased

* Corresponding author. Tel.: +49 431 880 2091.
E-mail address: wbensch@ac.uni-kiel.de (W. Bensch).

0040-6031/$ – see front matter © 2006 Elsevier B.V. All rights reserved.
doi:10.1016/j.tca.2006.11.006

steadily delivering a wide variety of compounds with the following cations: diammonium [19], ethylenediammonium [20], *N*-methylethylenediammonium, monoisopropylammonium, *N*, *N*-dimethyl-1,3-propane-diammonium, 1,4-butanediammonium [21], 1,3-propanediammonium, and *N*,*N*,*N*′,*N*′-tetramethylethylenediammonium [22], piperazine, tris(2-aminoethyl)amine [23], 1,4-dimethylpiperazinium [24]. The main objective of the investigations of these samples was to characterize the crystal arrangement and the influence of N–H···S interactions onto the geometry and bonding properties in the WS_4 moiety.

In a previous contribution the thermal decomposition pathways of tetraalkylammonium tetrathiomolybdates were reported [25]. In our ongoing work we investigated the analogous tetraalkylammonium tetrathiotungstates, $(R_4N)_2WS_4$ (R changes from methyl to heptyl) and the results of the experiments are presented here.

2. Experimental details

2.1. Preparation of $(R_4N)_2WS_4$ starting materials

The synthesis of the tetralkylammonium salts $(R_4N)_2WS_4$ has been reported by McDonald et al. [26] and by Alonso et al. [27]. The last method was used here in a modified version.

2.2. Synthesis of tetramethyl, tetraethyl and tetrapropylammonium thiotungstates

Fresh prepared $(NH_4)_2WS_4$ (1.4 mmol) was dissolved in water (30 mL) with stirring. 2.8 mmol of $(R)_4NBr$ (R = C1 = tetramethyl, C2 = tetraethyl, and C3 = tetrapropyl) was dissolved in NaOH (2.8 mmol) and 10 mL water with stirring. Both solutions were mixed and stirred for 30 min, then kept undisturbed over ice. Yellow crystals precipitated overnight with 80% yield. Cold water and ethanol were used for washing. These compounds are air stable for a long time.

2.3. Synthesis of tetrabutyl, tetrapentyl, tetrahexyl, and tetraheptylammonium thiotungstates

An aqueous solution of fresh $(NH_4)_2WS_4$ (0.7 mmol, 10 mL) was added to an aqueous solution of $(R)_4NBr$ (for R = C4 = tetrabutyl, C5 = tetrapentyl) (1.4 mmol, 20 mL), then stirred for 30 min. For R = C6 = tetrahexyl and C7 = tetraheptyl the solution was obtained in 10 mL water and 10 mL ethanol. Yellow powders precipitated with 80% yield and were stored under static vacuum over P_2O_5.

2.4. Methods and materials

DTA–TG and measurements coupled with mass spectrometry (MS) were performed using a NETZSCH STA-409CD device with Skimmer coupling, equipped with a BALZERS quadrupole mass spectrometer QMA 400 (max. 512 amu). For DTA–TG experiments alumina crucibles were used under a dynamic nitrogen atmosphere (flow rate: 75 mL/min, purity 5.0). In some cases the first derivative of the TG curve was used to confirm a thermal event. The TG curve of an empty crucible was measured under the same experimental conditions and the effects of gas flow and buoyancy were corrected automatically with the evaluation software. DTA–TG–MS measurements were performed under a dynamic helium atmosphere (flow rate: 50 mL/min, purity 5.6) in the analog scan mode. Heating rate of 4 K/min was applied in DTA–TG and MS coupled experiments up to 350 °C. The National Institute of Standards and Technology (NIST) (http://webbook.nist.gov/chemistry) data were used for comparison with the spectra obtained. Note that only one example is presented in the manuscript but all spectra are available as supplementary materials. DSC experiments were performed with a NETZSCH DSC 204 Phoenix device using aluminium crucibles pressed with an aluminium lid and also in sealed glass ampoules filled with argon. Protective atmosphere of nitrogen (30 mL/min) was applied. X-ray powder diffraction (XRPD) and in situ thermodiffractometry was performed on a STOE STADI-P instrument equipped with a graphite-high-temperature oven. The collected data were processed with the STOE WIN "X^{POW}" software. Chemical elemental analyses were performed on a HERAEUS CHN-O RAPID combustion analyzer, using zinc sample holders with 2–3 mg pro sample, heated up to 1000 °C under oxygen atmosphere. Scanning electron microscopy (SEM) and energy dispersive X-ray analysis (EDX) were performed with a Philips ESEM XL 30 scanning electron microscope.

3. Results

3.1. Elemental analysis

The data of the chemical analyses agree well with the chemical composition of the starting materials. These data are summarized together with the composition of the final decomposition products in Table 1. The carbon content increases gradually with the size of the alkyl group (2.02 wt% for C1 up to 11 wt% for C6). The hydrogen and nitrogen contents also increase from C1 to C7 alkyl precursors (0–1.1 wt% for H, 0.46 to 0.73 wt% for N). It is remarkable that the C/H ratio in the decomposition products for C1 to C5 educts remains more or less identical suggesting that these elements may exist combined as CH groups which remain trapped between the WS_2 layers or adsorbed on its surface. The W/S ratio is about 2 for C1–C5 in contrast to the C6 and C7 derived materials containing significantly less sulfur. However, in the last two materials the carbon and hydrogen content is very large and the nature of the incorporated C and H is not fully understood. But according to results presented in the literature one can assume that C partially substitutes S in WS_2 (see also below). In general, the size of the tetraalkylammonium cation influences the composition of the final decomposition product.

3.2. DTA–TG–DTG–MS characterization

3.2.1. Tetramethylammonium and tetraethylammonium thiotungstate $((CH_3)_4N)_2WS_4$ and $((CH_3CH_2)_4N)_2WS_4$

The thermal decomposition of $((CH_3)_4N)_2WS_4$ and $((CH_3CH_2)_4N)_2WS_4$ (Fig. 1) occurs in one step with 43.2%

Table 1
Data of chemical analysis, weight loss and thermal events for $(R_4N)_2WS_4$

R	Weight (%)	C (%)	H (%)	N (%)	S (%)	Composition	T_p (°C); T_e (°C)
Methyl		20.73	5.10	5.80	27.84		
	−43.2	20.87	5.21	6.08	27.86	$WS_{2.09}C_{0.43}N_{0.08}$	285; 265
		2.02	0.0	0.46	26.05		
Ethyl		32.96	6.93	4.89	22.10		
		33.57	6.98	4.89	22.4		
	−52	4.63	0.27	0.41	23.56	$WS_{1.9}C_{0.99}N_{0.07}H_{0.69}$	61, 245; 235
Propyl		42.08	8.25	4.04	18.86		
	−60.4	42.13	8.18	4.09	18.74	$WS_{2.01}C_{1.24}N_{0.11}H_{1.16}$	101, 178, 282; 170, 273
		5.64	0.44	0.59	24.25		
Butyl		42.88	8.14	3.11	14.13		
		48.25	9.04	3.51	16.10		
	−65.2	5.77	0.43	0.39	24.0	$WS_2C_{1.28}N_{0.07}H_{1.14}$	165, 205, 264, 326; 159, 256, 309
Pentyl		51.01	9.30	2.93	13.01		
	−69.3	52.85	9.68	3.08	14.10	$WS_{2.08}C_{1.22}N_{0.04}H_{1.13}$	117, 173.5, 227, 236, 258, 300; 168
		5.51	0.42	0.24	25.0		
Hexyl		55.83	10.23	2.69	10.5		
		56.48	10.19	2.74	12.56		
	−73.2	9.1	0.96	0.47	17.93	$WS_{1.43}C_{1.94}N_{0.08}H_{2.48}$	169, 253; 160, 247
Heptyl		59.2	11.03	2.53	10.86		
	−73.8	58.55	11.83	2.43	11.16	$WS_{1.61}C_{2.49}N_{0.14}H_{2.97}$	156, 250, 288; 146, 264
		11	1.1	0.73	19		

Chemical composition: first line, experimental values; second line, calculated values, third line, after decomposition.

mass loss for the first and 52% for the second compound. The experimental weight changes are less than expected for the formation of WS_2 (theo: 46% for C1 and 56.6% for C2). The differences between the values can be explained on the basis of chemical analysis (Table 1). The thermal degradations are accompanied by strong endothermic peaks (T_p = 285 °C, T_e = 265 °C for C1 and T_p = 245 °C, T_e = 235 °C for C2). Interestingly, the onset of thermal decomposition of $((CH_3)_4N)_2WS_4$ occurs at a significantly higher temperature (240 °C) than that of the second compound (150 °C). A thermal event at 61 °C observed for $((CH_3CH_2)_4N)_2WS_4$ was studied with DSC and XRD and the results are discussed below. $((CH_3)_4N)_2WS_4$ decomposes at slightly higher temperature than $(NH_4)_2WS_4$ (T_p = 252 °C [28]). In contrast to the ammonium compound no WS_3 is formed as an intermediate during the decomposition of C1 [29,30]. We note that for organic ammonium thiotungstates like $(pipH_2)WS_4$ and $(trenH_2)WS_4$ also a one step decomposition was reported [23]. According to the chemical analysis the C content in the decomposition product of C2 is larger than for C1.

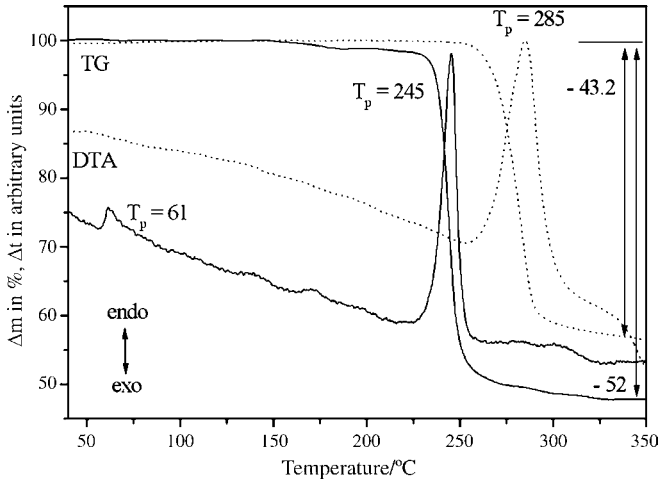

Fig. 1. DTA, TG plot of $[(methyl)_4N]_2[WS_4]$ = dash line and $[(ethyl)_4N]_2[WS_4]$ = solid line. Temperature in °C, mass loss in %.

In the mass spectrum recorded at 290 °C during decomposition of $((CH_3)_4N)_2WS_4$ the most intense signals are from the intact ions of tri-methylamine (m/z = 59) and dimethyldisulfide (m/z = 94). In the MS spectrum of C2 recorded at 244 °C again the intact ions of tri-ethylamine (m/z = 101) and diethyldisulfide (m/z = 122.1) molecules yield the most intense peaks. In both MS spectra the fragmentation patterns of the molecules matches well with the patterns seen in the NIST database for these molecules.

3.3. Tetrapropylammonium thiotungstate, $((CH_3(CH_2)_2)_4N)_2WS_4$

The DTA–TG curves show two decomposition steps and three endothermic events (Fig. 2). The first peak (T_p = 101 °C) represents a phase transition (see below). Thermal decomposition starts at 147 °C showing a strongest endothermic peak at 176 °C (T_e = 178 °C) and a second at 282 °C (T_e = 273 °C). The total mass loss (41.3% and 19.1% for the two steps) is less than expected for the formation of WS_2. Compared to the C1 and C2 compounds the residual C content is larger (Table 1). The results of the MS experiments clearly show the emission of

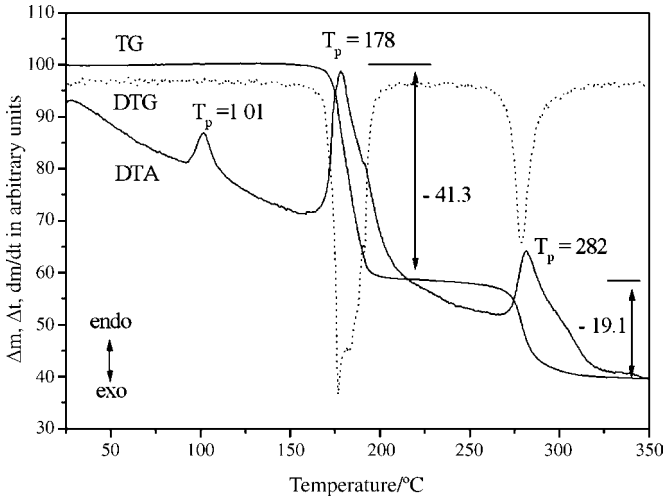

Fig. 2. DTA, TG and DTG plot of $[(propyl)_4N]_2[WS_4]$. Temperature in °C, mass loss in %.

ions of intact tri-propylamine ($m/z = 143$) and dipropyldisulfide ($m/z = 150$) as the main masses, and the fragmentation patterns of these to molecules.

3.3.1. Tetrabutylammonium thiotungstate, $((CH_3(CH_2)_3)_4N)_2WS_4$

The thermal degradation occurs in a wide temperature range (130–330 °C) with two mass losses, which are accompanied by four endothermic peaks (Fig. 3). In the first step the mass is reduced by 44.6% joined to two endothermic peaks, $T_p = 165$ °C ($T_e = 159$ °C) and $T_p = 205$ °C. In the second step the mass is reduced by 20.6% with one endothermic peak ($T_p = 264$ °C, $T_e = 256$ °C). Interestingly, an exothermic event at $T_p = 326$ °C ($T_e = 309$ °C) occurs which may be caused by structural rearrangements within the decomposition product. Like for the other compounds a remarkable difference between experimental (65.2%) and theoretical values for WS_2 formation (68.8%) is observed, and the difference can be explained on the basis of C, H, and N in the final product. MS data show the emission

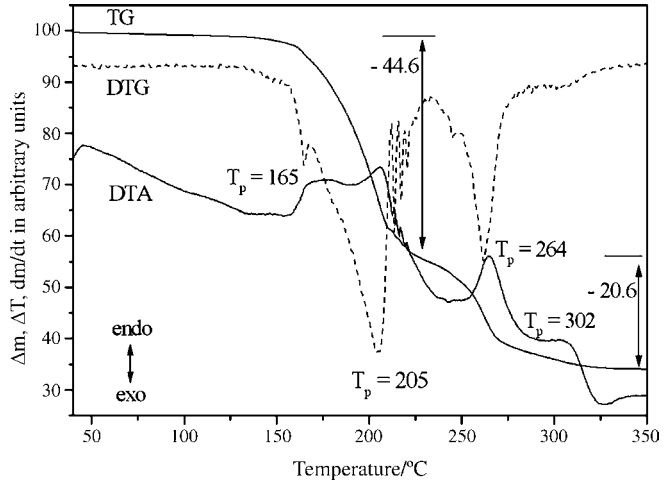

Fig. 3. DTA, TG and DTG plot of $[(butyl)_4N]_2[WS_4]$. Temperature in °C, mass loss in %.

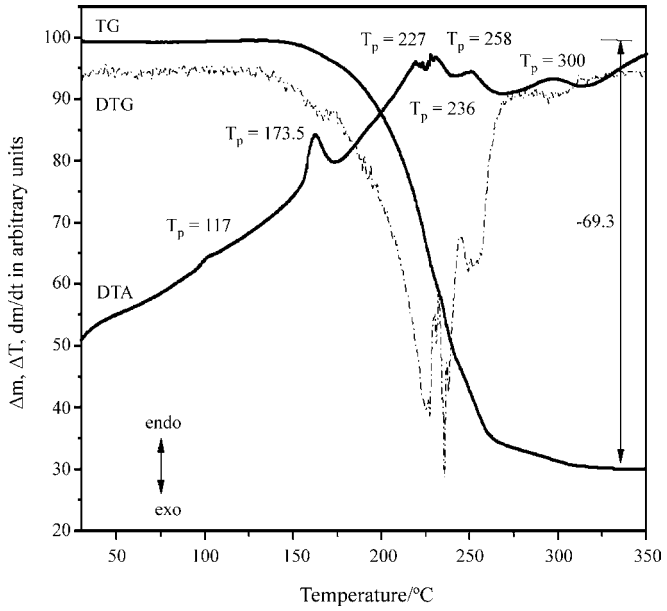

Fig. 4. DTA, TG and DTG plot of $[(pentyl)_4N]_2[WS_4]$. Temperature in °C, mass loss in %.

of tri-butylamine ($m/z = 185$) and dibutyldisulfide ($m/z = 178$) molecule during both weight change steps.

3.3.2. Tetrapentylammonium thiotungstate, $((CH_3(CH_2)_4)_4N)_2WS_4$

Several thermal events are observed in the DTA curve (Fig. 4). The first peak ($T_p = 117$ °C) corresponds to a phase transition (see below). The decomposition step extends from 135 to 330 °C containing four endothermic peaks ($T_p = 173.5$, 227, 236, and 258 °C). In the MS curves in this temperature range tri-pentylamine ($m/z = 227$), dipentyldisulfide ($m/z = 206$) and the fragmentation products of the two molecules are detected. A weak endothermic event at 300 °C in the DTA curve may be due to structural rearrangements of the degraded product. The calculated mass loss for WS_2 formation (72.6%) is larger than the experimental value of 69.3%. Again, the difference is due to C, H, N in the residue (Table 1).

3.3.3. Tetrahexylammonium and tetraheptylammonium thiotungstate $(CH_3(CH_2)_5)_4N)_2WS_4$ and $((CH_3(CH_2)_6)_4N)_2WS_4$

Both compounds decompose within a broad single step (Fig. 5) in the temperature ranges 140–337 °C (C6) and 160–343 °C (C7). In the DTA curve of C6 a very weak endothermal peak is located at $T_p = 169$ °C and an intense signal at $T_p = 253$ °C. The DTA trace of C7 shows a weak endothermic peak ($T_p = 156$ °C) which is discussed below and a complex endothermic event with two maxima at $T_p = 250$ °C and $T_p = 288$ °C. It is remarkable that in the decomposition products the S contents are significantly reduced and the amount of C increased. This observation suggests that S could be replaced by C as already reported by Berhault *et al.* from studies of the interaction of carbon with transition metal sulfides in the activation process of catalysts [31]. The total mass loss for C6

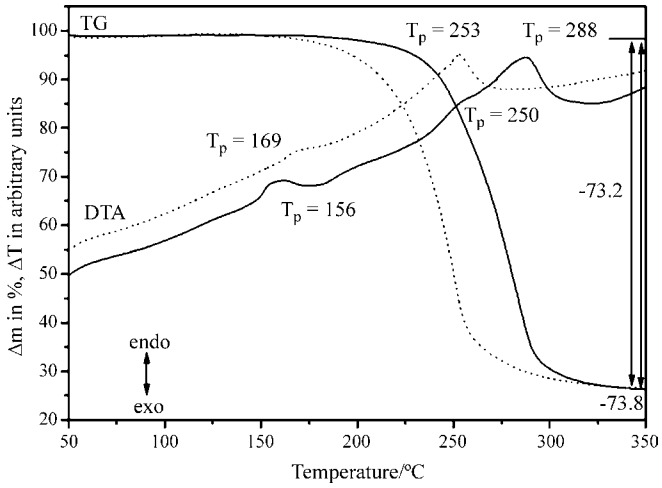

Fig. 5. DTA, TG plot of: $[(hexyl)_4N]_2[WS_4]$ = dash line and $[(heptyl)_4N]_2[WS_4]$ = solid line. Temperature in °C, mass loss in %.

(73.2%) is low compared to 76.6% calculated for WS_2 formation. The same tendency is seen for C7 with total mass loss of 73.8% versus 76.98% calculated. The MS experiments clearly indicate that intact tri-hexylamine (m/z = 269) and dihexyldisulfide (m/z = 234.2) ions are emitted (C6) while the elimination of tri-heptylamine (m/z = 311) and diheptyldisulfide (m/z = 262) is detected for C7. We note that like in the former cases the fragmentation patterns of the tri-alkylamine and diaminsulfide molecules are in agreement with data reported in the NIST database.

3.4. Scanning electron microscopy

In the SEM micrograph of the C1 decomposition product long faceted particles with a rough surface are seen, similar to the WS_2 particles obtained from ammonium thiotungstate (ATT). Therefore, the decomposition process is suggested to be topotactic, i.e. the morphology of the precursor material is maintained [25,32]. The morphology of the C2 decomposition material shows no cavities in contrast to the analogous Mo sample morphology [25]. An interesting morphology occurs in the decomposition product of the C3 precursor (Fig. 6). Needle like particles with size between 30 and 45 μm are observed which are amorphous according to the XRPD pattern. It is documented in the literature that decomposition products of thiotungstates yield products with a more pronounced morphology than the thiomolybdates analogues [33]. For the C4 precursor a partially molten surface is observed while C5 and C6 decomposition materials (Fig. 7) yield solid pieces. Only for the heptyl sample (Fig. 8) the decomposition product shows cavities like those obtained for the Mo analogue [25]. The R_4N molecules are widely used as 'templates' for zeolites and mesoporous material syntheses [34]. The 'templates' stabilize voids inside the solid structure that are proportional to the size of the alkyl group in the molecule. The WS_2 material generated from the heptyl precursor may be considered as an amorphous mesoporous material like that reported before for Mo compounds [25,35], or it may be called amorphous zeolite as claimed by Alonso et al. [36]. Every member of the Mo analogues family developed surface porosity showing a gradual increase of pore sizes according to the alkyl precursor chain length, whereas the W educts produced more compact decomposition products.

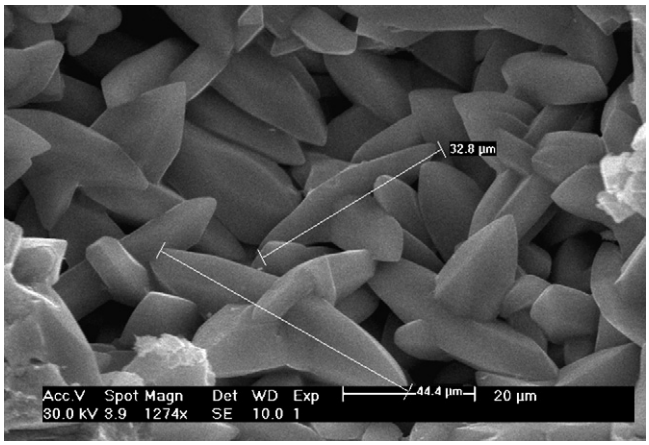

Fig. 6. SEM image of the thermal decomposition product of $[(propyl)_4N]_2[WS_4]$.

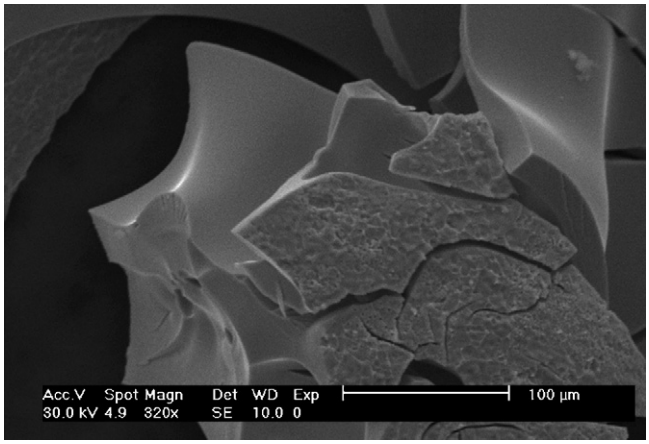

Fig. 7. SEM image of the thermal decomposition product of $[(hexyl)_4N]_2[WS_4]$.

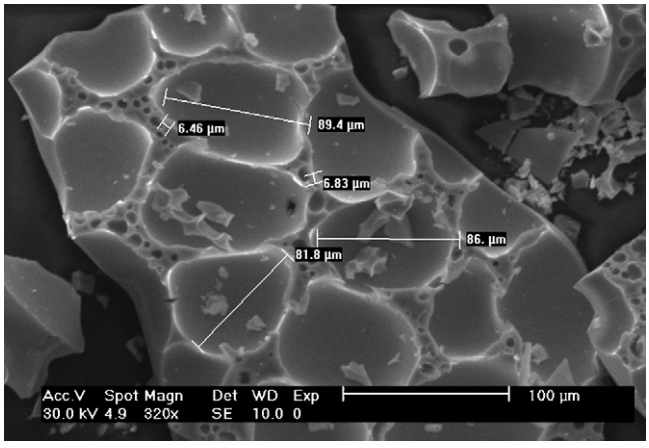

Fig. 8. SEM image of the thermal decomposition product of $[(heptyl)_4N]_2[WS_4]$.

3.5. DSC experiments and X-ray powder diffraction

The DSC trace of the tetraethyl sample exhibits an endothermic event (T_p = 64 °C) in the heating curve and an exothermic peak (T_p = 29 °C) in the cooling curve (Fig. 9). After this treatment the XRPD shows reflections of a new crystalline phase (Fig. 10), which was further supported by thermodiffractometry experiments (Fig. 11). In order to follow the reversibility of this structural phase transition another DSC experiment was undertaken. In the DSC curves an endothermic event occurs (T_p = 34 °C, T_e = 29 °C) which matches not with the event seen during the first heating experiment, meanwhile the second cooling curve shows an exothermic peak (T_p = 29 °C, T_e = 23 °C) identical to that registered in the first cooling curve. Obviously, the pristine material (I) undergoes an irreversible structural phase transition to a new phase (II), and this second phase shows a reversible structural phase transition to phase (III). Transition temperatures of compounds R_4NBF_4 (R = C1–C4) have been observed at 63 °C for C2 [37]. The C3 sample shows a similar behaviour with that of the tetraethyl compound with a broad and intense endothermic signal (T_p = 88 °C, T_e = 78 °C) in the heating curve and an exothermic peak (T_p = 53 °C, T_e = 45 °C) in the cooling curve (Fig. 9). The XRPD pattern of the material after the DSC experiment exhibits reflections of a new crystalline phase (Fig. 12). Again, the structural phase transition is confirmed by thermodiffractometry measurements (Fig. 13). The reversibility of the phase transition was probed by a second DSC measurement, which displays an endothermic event (T_p = 91 °C, T_e = 74 °C) during heating and an exothermic peak (T_p = 51 °C, T_e = 44 °C) during cooling. Like in the previous case this material (I) transforms to a new phase (II), which reversibly undergoes a phase transition into a third phase (III). Interestingly

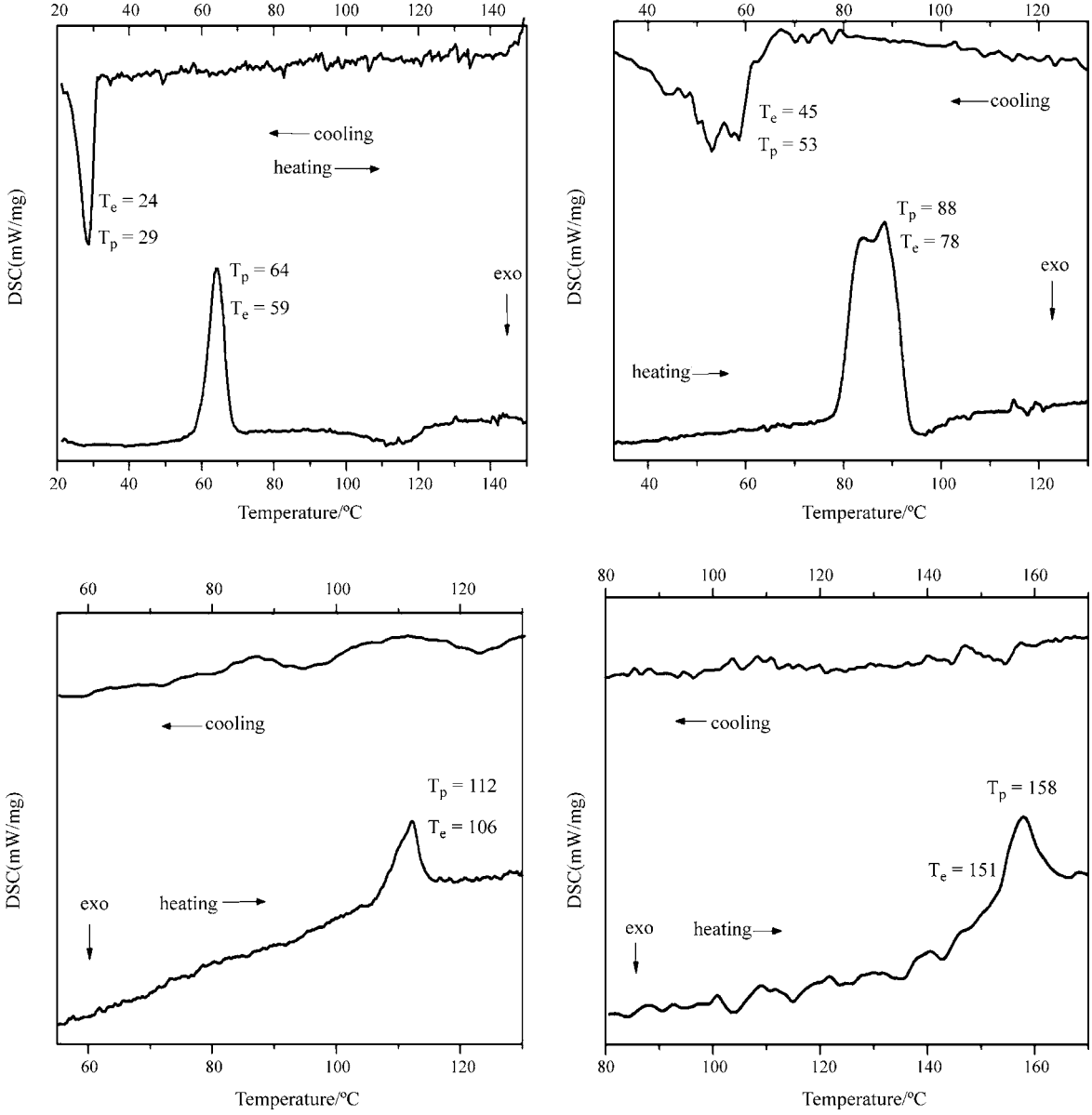

Fig. 9. DSC traces of the ethyl (top left), propyl (top right), pentyl (bottom left) and heptyl (bottom right) compounds $[(R)_4N]_2[WS_4]$.

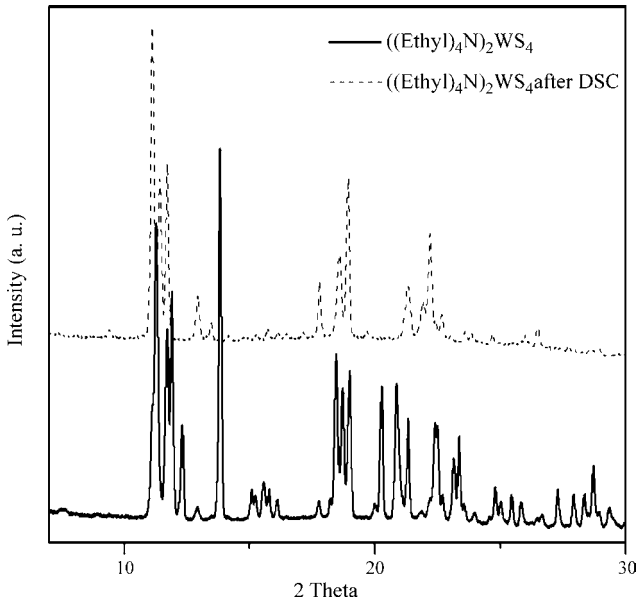

Fig. 10. Powder patterns of tetraethylammonium tetrathiotungstate, before and after the DSC experiment. *Note*: the sample was heated up to 150 °C.

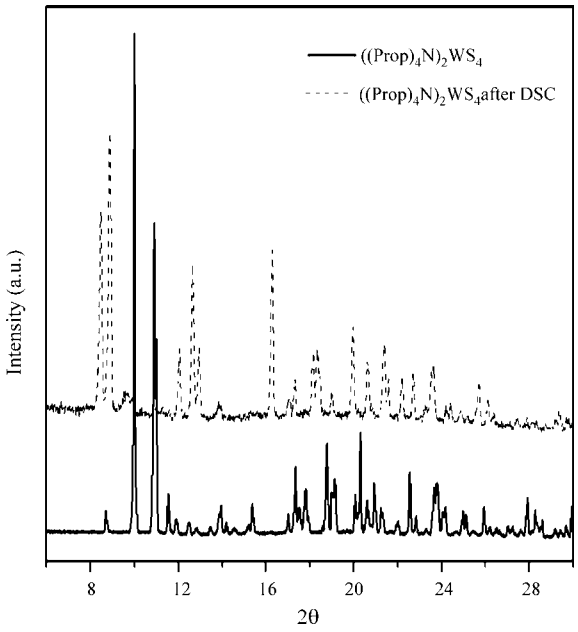

Fig. 12. Powder patterns of tetrapropylammonium tetrathiotungstate, before and after the DSC experiment. *Note*: the sample was heated up to 150 °C.

no phase transition is observed for the C4 precursor in contrast to the Mo analogue sample, which showed a transition at 113 °C [25].

In the DSC experiment of the tetrapentyl compound (Fig. 9) an endothermic peak (T_p = 112 °C) occurs but there is no signal in the cooling curve. According to the X-ray powder pattern collected after the treatment a new phase is formed (Fig. 14). Contrary to the Mo analogue [25], the tetrahexyl thiotungstate sample shows no thermal event in the DSC curve up to 150 °C. Finally, the C7 sample behaves similarly to the molybdenum analogue. In the DSC heating curve (Fig. 9) an intense endothermic peak is detected (T_p = 158 °C) but no peak occurs in the cooling curve indicating the irreversibility of this effect. The powder pattern of a sample heated to 150 °C (Fig. 15) shows a broad modulation of the background in the region of the pristine material and several new reflections at higher scattering angles suggesting a partial decomposition. When the sample is heated to 170 °C an amorphous material is obtained and in the XRPD only broad and featureless modulations occur. The product looks like

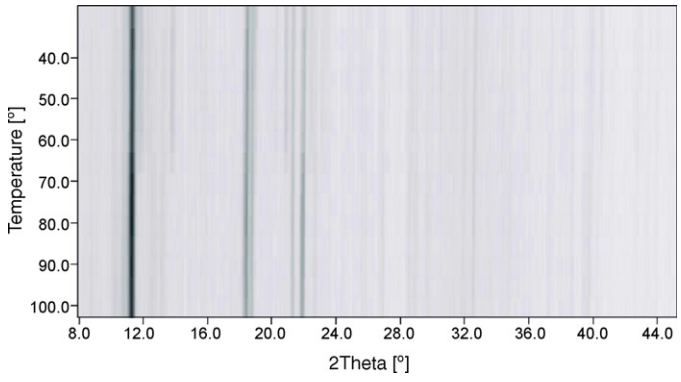

Fig. 11. Powder patterns of the in situ X-ray diffraction experiments of tetraethylammonium tetrathiotungstate.

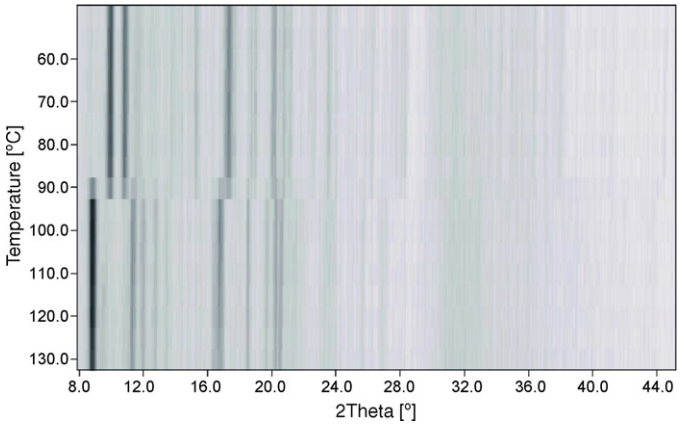

Fig. 13. Powder pattern of the in situ X-ray diffraction experiments of tetrapropylammonium tetrathiotungstate.

a glass and the chemical analysis reveals a loss of about 11 wt% C and 2.2 wt% H. It can be assumed that incongruent melting occurs at the beginning of the decomposition process, in contrast to the Mo analogue, which showed a melting point with no change of the chemical composition [25].

4. Discussion

Our recent study about the thermal decomposition of tetraalkylammonium tetrathiomolybdates revealed an increasing complexity of the thermal reactions with increasing alkyl chain lengths. During the thermal degradation tri-alkylamines and dialkyldisulfides were eliminated and for some samples low-temperature structural phase transitions were observed [25]. The tetraalkylammonium thiotungstates show a similar behaviour suggesting that the decomposition processes are very similar. For all samples the MS data reveal that intact tri-alkylamine and

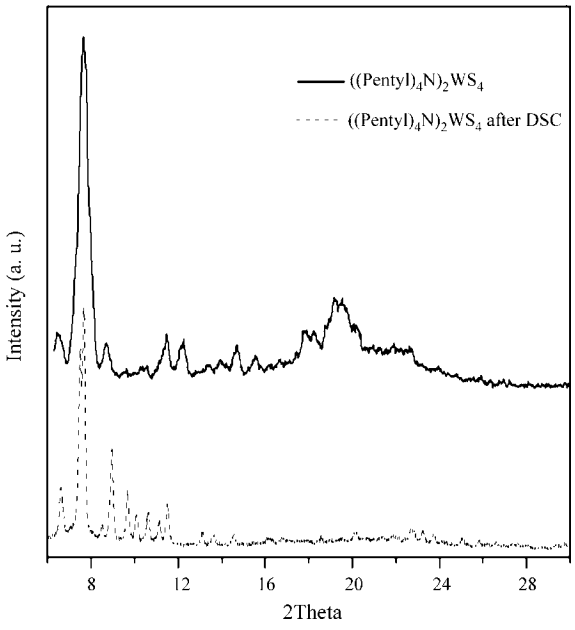

Fig. 14. Powder patterns of tetrapentylammonium tetrathiotungstate before and after the DSC experiment. *Note*: the sample was heated up to 150 °C.

dialkyldisulfide molecules are the main species emitted during thermal decomposition. All experimental MS data display the fragmentation patterns of these molecules as is evidenced by a careful comparison with the data found in the NIST database. The MS traces of the tetrapropyl precursor are shown as an example in Fig. 16. The formation of dialkyldisulfide molecules can be envisaged by the reaction of intermediate formed alkyl radicals with two S atoms from the $(WS_4)^{2-}$ anion. Therefore, a general decomposition pathway can be represented as

$$(R_4N)_2WS_4 \rightarrow 2R_3N + R_2S_2 + WS_{2-n}C_xN_yH_z$$

with values for n, x, y, and z depending on the actual composition of the precursor material (compare Table 1). In order

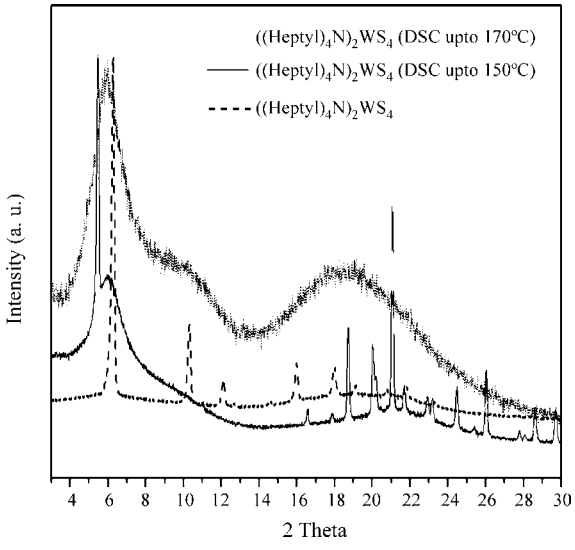

Fig. 15. Powder patterns of tetraheptylammonium tetrathiotungstate before and after DSC experiments up to 150 and 170 °C.

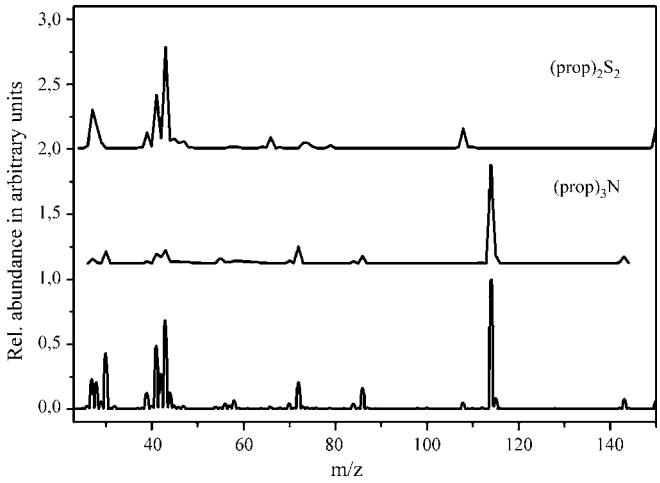

Fig. 16. Mass spectrum of $[(propyl)_4N]_2[WS_4]$ scanned at 183 °C. Note: the top two traces were taken from http://webbook.nist.gov/chemistry.

to explain this reaction a nucleophilic bimolecular substitution (S_N2) mechanism is most likely [25]: a nucleophilic attack from one anionic sulfur atom to the α carbon atom in the ammonium ions gives tri-alkylamine and dialkyldisulfide as products [38].

The XRPD patterns of all decomposition products show a high dispersion of the phases with very low layer stacking and no reflections of crystalline carbon or tungsten carbides are seen indicating that no segregation of C or formation of a carbide occurs in the final product. Fig. 17 shows a comparison of the powder patterns of C5, C6 and C7 decomposition products with that of 2H-WS_2. Amorphous tungsten disulfide (a-WS_2) is formed up to C5 derived materials, which is in agreement with the observation made by Liang et al. [39]. The XRPD of the C6 and C7 decomposition products are typical for highly dispersed small particles with a low layer stacking. In view of results presented by Berhault et al. [40] it can be assumed that S atoms at the edges of WS_2 platelets are replaced by C atoms and $WS_{2-x}C_x$ materials are formed. According to these evidences published in [40] C stabilizes texturally sulfide particles keeping the crystallites smaller and less stacked. Furthermore, all decomposition

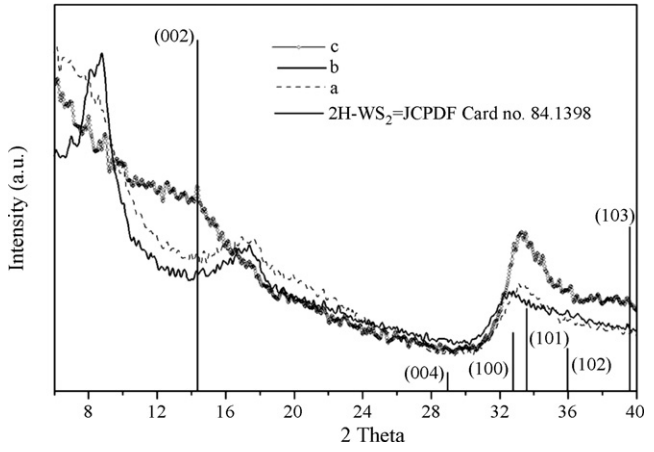

Fig. 17. Powder patterns of $[(R)_4N]_2[WS_4]$ after thermal decomposition up to 350 °C, R = (a) heptyl, (b) hexyl and (c) pentyl. Vertical bars indicate the positions of reflections of crystalline WS_2.

products were characterized with IR spectroscopy and no hints were found for the presence of undestroyed organic molecules, i.e., no signals of C–H or C–N vibrations were seen.

The hexyl and heptyl decomposition products show W/C and W/H ratios larger than the W/S stoichiometric ratio (Table 1). A similar observation was made for the analogous Mo compounds [25], but the carbon content was not as large as in the present decomposition products [25]. Another difference to the Mo samples is the observation that the W based decomposition products are more compact and only the precursor with the longest alkyl chain produces large cavities. The DSC results in combination with in situ X-ray diffraction highlight the complex thermal behaviour of these materials. The tetraethyl and tetrapropyl samples undergo structural phase transitions at low temperatures, which may be due to conformational motion and/or disorder of the alkyl chains. Such a disorder is seen in the crystal structure of the tetrapropyl tetrathiotungstate at room temperature [41]. Similar transitions were reported in the literature for tetraethyl and tetrapropylammonium tetraclorozincates [42]. The results of our study indicate that the two tetraalkylammonium thiotungstates obtained by solvent route are metastable forms that transform into the thermodynamically more stable materials upon heating.

For the tetrabutylammonium compound the most extended decomposition process (110–330 °C) is observed, but no phase transition occurs. For tetrabutylammonium iodide a glass transition was reported at 230 K [43]. The low decomposition temperature may be due to the fact that the material melts just before thermal degradation starts. Similarly for the tetraalkylammonium tetrafluoroborate series with C1–C4, the earliest melting point has been observed for C4 compound [37]. The tetrapentyl sample is irreversibly transformed into a new compound at 112 °C, a different behavior compared with the Mo analogue [25]. No phase transition is observed for the tetrahexyl sample, in contrast to what was found for the analogous Mo sample. The tetrahexyl and tetraheptyl precursors show both weak endothermic peaks at around 160 °C, followed by more complex endothermic events. The corresponding X-ray powder patterns evidence that the products are amorphous immediately after the decomposition process starts. The disorder and motion in crystals and mesophases of tetrahexylammonium iodide was studied based on entropy changes during the phase transition concluding that the mesophase is likely a conformational disordered crystal [44]. The disordered crystals may be quenched to glasses as it has been observed by quenching of the present tetraheptyl compound at 150 °C.

5. Summary

The tetraalkylammonium thiotungstates, $(R_4N)_2WS_4$, with R = methyl to heptyl undergo thermal decomposition reactions very similar to the analogous Mo samples. The elimination of tri-alkylamines and dialkyldisulfides is accompanied by endothermic peaks in DSC and DTA curves. All samples decompose without formation of WS_3 as an intermediate. The composition of the final products is affected by the alkyl chain length: samples from methyl through pentyl yield WS_2, whereas the hexyl and heptyl precursors decompose to carbon supported tungsten sulfides because the carbon content is higher than the sulfur content. Previous studies presented evidences that the surface of the active phase under real hydrotreating conditions presents a carbidic like nature. Therefore, thermal decomposition of starting materials with long alkyl chains offer the possibility to prepare catalysts with a desired structural C content. We note that tetraheptyl thiotungstate was used as starting material for the preparation of active WS_2 catalysts [45]. In this study the precursor was not decomposed prior to the catalytic test but was applied under HDS conditions yielding in situ formed active WS_2 material containing a large amount of carbon. Like for the molybdenum analogues a general decomposition reaction mechanism is proposed following a nucleophilic bimolecular substitution (S_N2) mechanism yielding tri-alkylamines and dialkyldisulfides as eliminated products. The morphology of the final decomposition products shows no tendency to develop porous materials. This observation is in contrast to the findings for the analogous Mo samples. A highly interesting result is that several compounds undergo phase transitions to more stable polymorphs. These new modifications are then reversibly transformed into a new modification at elevated temperatures. X-ray diffraction analyses of the final products demonstrate that amorphous WS_2 is obtained up to the tetrapentyl material, and with C6 and C7 precursors S-poor products are developed which may be better described as carbosulfide phases.

Acknowledgements

The authors thank C. Teske for fruitful discussions. The financial support by the Deutsche Forschungsgemeinschaft DFG (project: BE 1653/11-2) is gratefully acknowledged.

References

[1] R.R. Chianelli, M. Daage, Adv. Catal. 40 (1994) 7.
[2] M. Yamada, Catal. Surv. Jpn. 3 (1999) 3.
[3] D.S. Thakur, B. Delmon, J. Catal. 91 (1985) 308.
[4] M. Breysse, J.L. Portefaix, M. Vrinat, Catal. Today 10 (1991) 489.
[5] F. Luck, Bull. Soc. Chim. Belg. 100 (1991) 781.
[6] B. Delmon, Catal. Lett. 22 (1993) 1.
[7] R.R. Chianelli, T.A. Pecoraro, US Patent 4,508,847 (1985).
[8] M. Zdrazil, Catal. Today 3 (1988) 269.
[9] G. Alonso, M. Del Valle, J. Cruz, A. Licea-Claverie, V. Petranovskii, S. Fuentes, Catal. Lett. 52 (1998) 55.
[10] F. Pedraza, S. Fuentes, Catal. Lett. 65 (2000) 107.
[11] G. Alonso, M. Del Valle, J. Cruz, A. Licea-Claverie, V. Petranovskii, S. Fuentes, Catal. Today 43 (1998) 117.
[12] G. Alonso, V. Petranovskii, M. Del Valle, J. Cruz-Reyes, A. Licea-Claverie, S. Fuentes, Appl. Catal. A: Gen. 197 (2000) 87.
[13] K. Inamura, R. Prins, J. Catal. 147 (1994) 515.
[14] M. Sun, T. Bürgi, R. Cattaneo, R. Prins, J. Catal. 197 (2001) 172.
[15] M. Sun, M.E. Bussel, R. Prins, Appl. Catal. A 216 (2001) 103.
[16] M. Sun, P.J. Kooyman, R. Prins, J. Catal. 206 (2002) 368.
[17] V. Schwartz, M. Sun, R. Prins, J. Phys. Chem. B. 106 (2002) 2597.
[18] G. Alonso, J. Espino, G. Berhault, L. Alvarez, J.L. Rico, Appl. Cat. A 266. (2004) 29.
[19] B.R. Srinivasan, M. Poisot, C. Näther, W. Bensch, Acta Crystallogr. E 60 (2004) i136.
[20] B.R. Srinivasan, S.N. Dhuri, C. Näther, W. Bensch, Acta Cryst. E 58 (2002) m622.

[21] B.R. Srinivasan, S.N. Dhuri, C. Näther, W. Bensch, Monatshefte Chemie 137 (2006) 397.
[22] B.R. Srinivasan, S.N. Dhuri, C. Näther, W. Bensch, Acta Crystallogr. C 59 (2003) m124.
[23] B.R. Srinivasan, S.N. Dhuri, M. Poisot, C. Näther, W. Bensch, Z. Anorg. Allg. Chem. 631 (2005) 1087.
[24] B.R. Srinivasan, S.N. Dhuri, C. Näther, W. Bensch, Acta Crystallogr. E 59 (2003) m681.
[25] M. Poisot, W. Bensch, S. Fuentes, G. Alonso, Thermochim. Acta 444 (2006) 35.
[26] J.W. McDonald, G.D. Friesen, L.D. Rosenhein, W.E. Newton, Inorg. Chim. Acta 72 (1983) 205.
[27] G. Alonso, G. Aguirre, I.A. Rivero, S. Fuentes, Inorg. Chim. Acta 274 (1998) 108.
[28] J. Espino, L. Alvarez, C. Ornelas, J.L. Rico, S. Fuentes, G. Berhault, G. Alonso, Catal. Lett. 90 (2003) 71.
[29] T.P. Prasad, E. Diemann, A. Müller, J. Inorg. Nucl. Chem. 35 (1973) 1895.
[30] A. Müller, E. Diemann, R. Jostes, H. Bögge, Angew. Chem. 93 (1981) 95.
[31] G. Berhault, L.C. Araiza, A.D. Moller, A. Mehta, R.R. Chianelli, Catal. Lett. 78 (2002) 81.
[32] K. Voorhoeve, J. Stuiver, J. Catal. 23 (1971) 228.
[33] M. Del Valle, M. Yanez, M. Avalos, S. Fuentes, in: M. Ocelli, R.R. Chianelli (Eds.), Hydrotreating Technology for Pollution Control, 1996, p. 47.
[34] K. Holmberg, J. Colloid Interf. Sci. 274 (2004) 355.
[35] G. Alonso, G. Berhault, F. Paraguay, E. Rivera, S. Fuentes, R.R. Chianelli, Mater. Res. Bull. 38 (2003) 1045.
[36] G. Alonso, M.H. Siadati, R.R. Chianelli, US Patent Application 20050032636.
[37] G. Zabinska, P. Ferloni, M. Sanesi, Thermochim. Acta 122 (1987) 87.
[38] J. March, Advanced Organic Chemistry: Reactions Mechanism and Structure, Mc Graw-Hill, Japan, 1968.
[39] K.S. Liang, R.R. Chianelli, F.Z. Chien, S.C. Moss, J. Non-Cryst. Solids 79 (1986) 251.
[40] G. Berhault, A. Mehta, A.C. Pavel, J. Yang, L. Rendon, M.J. Yacaman, L.C. Araiza, A.D. Moller, R.R. Chianelli, J. Catal. 198 (2001) 9.
[41] M. Poisot, C. Näther, W. Bensch, Z. Naturforsch 61b (2006) 1.
[42] R. Blachnick, C. Siethoff, Thermochim. Acta 278 (1996) 39.
[43] A. Xenopoulos, A.H. Narten, J. Cheng, B. Wunderlich, J. Non-Cryst. Solids 131 (1991) 113.
[44] J. Cheng, A. Xenopoulos, B. Wunderlich, Mol. Cryst. Liq. Cryst. 220 (1992) 127.
[45] G. Alonso, R.R. Chianelli, J. Catal. 221 (2004) 657.